

Article

Modeling of Induction Motor Direct Starting with and without Considering Current Displacement in Slot

Marina Konuhova 

Institute of Solid State Physics, University of Latvia, 8 Kengaraga, LV-1063 Riga, Latvia;
marina.konuhova@cfi.lu.lv

Abstract: This article presents a mathematical model of three-phase induction motor (IM) with a squirrel cage rotor and investigates its starting modes. Specifically, two scenarios are considered: direct starting of an IM and direct starting considering the current displacement effect in the rotor slots. Analyzing the starting modes of an IM without the use of automatic control systems is crucial for ensuring reliable, efficient, and safe operation of equipment across various industrial and commercial sectors. Understanding and accounting for the processes occurring during the starting mode of an IM allows for minimizing risks, enhancing energy efficiency, and reducing operational costs. This article details the mathematical modeling methods used for analyzing these starting modes and the results obtained from the modeling. These results were compared with data obtained experimentally, allowing for the assessment of the accuracy and reliability of the proposed model. The conducted research highlights the importance of considering current displacement in the rotor slots for accurate modeling and analysis of induction motor starting modes, particularly in capturing the differences in the amplitudes of the starting current and the faster transition to steady-state operation. Conclusions drawn from the comparison of modeling and experimental data provide valuable insights for the further development of control and operation methods for induction motors.

Keywords: induction motor; modeling; starting mode; current displacement in slot; transients



Citation: Konuhova, M. Modeling of Induction Motor Direct Starting with and without Considering Current Displacement in Slot. *Appl. Sci.* **2024**, *14*, 9230. <https://doi.org/10.3390/app14209230>

Academic Editor: Frede Blaabjerg

Received: 13 August 2024

Revised: 1 October 2024

Accepted: 3 October 2024

Published: 11 October 2024



Copyright: © 2024 by the author. Licensee MDPI, Basel, Switzerland. This article is an open access article distributed under the terms and conditions of the Creative Commons Attribution (CC BY) license (<https://creativecommons.org/licenses/by/4.0/>).

1. Introduction

An induction motor (IM) is an electrical machine designed to convert electrical energy into mechanical energy [1,2]. An AC induction motor consists of a fixed outer stator and a rotor that rotates inside, separated by an air gap. In a three-phase AC induction motor, the AC supply creates a naturally rotating magnetic field in the stator. This changing magnetic field induces an electromagnetic force (EMF) in the rotor, generating currents and magnetic fields within it. The interaction between the stator and rotor magnetic fields generates torque, causing the rotor to rotate [3].

The most widely used type of IM is the squirrel cage rotor motor. Its widespread use is due to several advantages over other types of motors: high reliability, the ability to operate directly from an AC power supply, ease of maintenance, simplicity in manufacturing, low cost, and the absence of mechanical contact with the stationary parts of the machine, which ensures durability and reduces maintenance costs [4].

Three-phase induction motors with squirrel cage rotors have several advantages over single-phase induction motors, particularly in terms of performance and application. Although both single-phase and three phase induction motors use squirrel cage rotors, three-phase motors are generally more efficient, can start heavier loads, and are better suited for industrial applications. Three-phase motors also provide smoother operation and greater reliability in high-power environments, making them more suitable for large-scale commercial and industrial use compared to their single-phase counterparts [3].

The main problem encountered when using an IM with a squirrel cage rotor is the direct starting of the motor. A significant drawback of the squirrel cage rotor is its low starting torque and high inrush current, which is several times higher than the nominal current

value. These factors can negatively impact the motor's operation and cause significant mechanical shocks [5–7].

The primary applications of induction motors (IMs) without automatic control include industrial installations where cost-effective and reliable solutions are necessary. In certain settings, such as small and medium enterprises, the decision not to use automatic control systems is often driven by cost-effectiveness and practicality rather than the size of the business itself [8]. Simple and robust IMs are commonly used to drive equipment such as pumps, fans, and conveyors in these situations [9]. This also applies to agricultural settings, where induction motors power machines without the need for automation, as the simplicity and reliability of these systems make them ideal [10]. In household and utility services, such as water supply compressors and ventilation systems [11], IMs often operate without complex control systems, as the demand for automation is minimal in these applications. Understanding the performance of IMs in such scenarios is critical to ensuring their reliability and efficiency in environments where automatic control is not utilized.

Research into the operating modes of IM is of significant importance, as evidenced by numerous ongoing studies in this area [12]. Understanding these modes is not only crucial for addressing starting characteristics but also for a wide range of issues, including fault detection and diagnosis. Current research focuses on fault detection in IMs [13–15], condition monitoring and practical diagnostics [16,17], and fault diagnosis based on current signature analysis [18,19]. Additionally, studies explore condition monitoring and diagnostics of rotor faults [20–23], broken bar detection [24–28], and fault detection based on the start-up current envelope [29]. These investigations complement the study of IM-starting characteristics by improving the overall efficiency of IM drives through flux and torque control, which remains a key area of research [30,31].

Also, the study of the operating modes of an IM plays a crucial role in optimizing its operation to reduce energy consumption [32]. Optimal management of operating modes and a deep understanding of the processes occurring within the motor contribute to increased energy efficiency. This is particularly important in situations where automatic control systems are absent. Knowledge of the electrical and thermal processes within the motor helps prevent emergency situations and ensures safe operating conditions [33].

Research and optimization of operating modes without the use of automatic control systems can significantly reduce operating and maintenance costs. Proper operation of the motor reduces expenses on maintenance and replacement of worn components, positively affecting the economic efficiency of equipment use [34].

The study of dynamic operating modes of the induction motor, taking into account electromagnetic transient phenomena caused by changes in the motor's state, is a highly relevant task in the modern practice of using low-inertia induction drives. Low-inertia induction drives refer to systems with reduced rotational inertia, which allows for faster acceleration and more responsive operation to changes in load or speed. These drives are particularly useful in applications where quick dynamic responses are required, such as robotics or precision machinery [35]. Direct starting, which involves applying full voltage to the motor, is the simplest and most cost-effective method of starting an IM [36]. It is also the most commonly used method for starting equipment, particularly in applications without automatic control systems, due to its simplicity and cost-effectiveness [37].

A deeper understanding of dynamic processes, such as electromagnetic transient phenomena, not only enhances the efficiency of the motor's operation but also improves its reliability. This, in turn, reduces the risk of accidents and extends the lifespan of the equipment, which is crucial for enterprises aiming for sustainable development and reduced operational costs. Thus, a comprehensive approach to studying the operating modes of the induction motor provides significant advantages, contributing to the overall efficiency and reliability of production processes.

To model IM-starting behavior, particularly in direct-start conditions, several mathematical models are commonly employed. These models range in complexity and accuracy,

depending on the level of detail they capture and the assumptions they make. The most commonly used mathematical models for simulating the start-up behavior of induction motors provide varying levels of insight, depending on the phenomena they are designed to represent [38,39].

One of the simplest methods for analyzing induction motor startup behavior is the steady-state equivalent circuit model, which represents the motor's stator and rotor characteristics using electrical resistances and inductances. While computationally efficient, it assumes steady-state conditions and ideal sinusoidal voltages, limiting its ability to capture dynamic processes during startup [40–42]. A more advanced approach is the dynamic D–Q model, which uses Park's transformation to simplify analysis by converting three-phase currents into two orthogonal components in a rotating reference frame. This model is effective for capturing transient phenomena, like inrush currents and torque oscillations, though it requires precise rotor parameters and balanced conditions [12,39,43,44]. Coupled magnetic circuit models represent the motor as multiple coupled circuits and are especially useful for simulating rotor bar currents during startup but require significant computational resources [45]. Space vector models simplify the analysis of induction motors by using complex vectors to represent the motor's electrical variables. This method provides a compact and efficient way to model motor dynamics during both steady-state and transient conditions. One of the main advantages of space vector models is their ability to reduce the number of differential equations required, making them computationally efficient while still capturing important transient behaviors [46,47].

Each model has its strengths and limitations, depending on the required details and available computational resources. Simpler models like the steady-state equivalent circuit may suffice for basic applications, while more advanced models like D–Q or space vector models are better suited for detailed startup simulations or real-time control [48].

Conventional mathematical models for induction motors typically assume a uniform current distribution in the rotor slots. This assumption overlooks the phenomenon of current displacement, where the current density varies along the height of the rotor slot due to changes in inductive reactance. As a result, conventional models tend to underestimate the starting current and overestimate the motor's acceleration during the direct-starting process. These inaccuracies can lead to significant discrepancies between predicted and actual motor behavior, particularly in high-power applications where precise control of starting dynamics is critical.

This paper presents a mathematical model of a three-phase induction motor (IM) with a squirrel cage rotor, focusing on the analysis of its direct-starting mode using a model in the $\alpha\beta$ coordinate system. Specifically, two models are analyzed: one that ignores current displacement in the rotor slots and one that accounts for it. Both models are used to study the direct starting of the motor and compare the dynamic characteristics in each case.

The chosen model is particularly effective in simulating the start-up behavior of the motor, including phenomena such as rotor acceleration and the interaction between stator and rotor flux linkages. By incorporating the effect of current displacement, the model provides a more accurate representation of the starting current and torque profiles. This allows for a detailed examination of how current displacement influences motor performance during start-up. The results obtained from the mathematical models are compared with experimental data to validate their accuracy and reliability.

2. Mathematical Model of the Induction Motor

To analyze the operation of an IM during transient processes, the choice of the electric motor's mathematical model is an important and often decisive factor. An efficient solution for such tasks involves using a mathematical model in orthogonal coordinates, where the primary variables are the voltages and currents of the electric machine.

In the first stage of modeling the dynamic operation regimes of an IM, conventional assumptions are traditionally applied. These assumptions enable the analysis of an ideal-

ized machine, rather than a real electric machine. The idealized machine is characterized by the following [49]:

1. No magnetic circuit saturation, hysteresis, or iron loss: this means that the magnetic materials in the motor are assumed to behave perfectly, without any energy losses or limits on how much magnetism they can handle;
2. No current displacement in winding copper: the flow of electric current in the motor's windings is assumed to be evenly distributed, without any irregularities caused by the changing frequency of the current;
3. Sinusoidal distribution of magnetic flux density and magnetizing forces in space: the magnetic field inside the motor is assumed to be smooth and evenly spread out, creating consistent forces that drive the motor;
4. Independence of winding leakage inductance from rotor position: the magnetic leakage, which is the small amount of magnetic energy that escapes from the windings, is assumed to stay the same regardless of the rotor's position;
5. Complete symmetry of windings: the windings (the coils of wire in the motor) are assumed to be perfectly balanced and identical, which simplifies the analysis.

The idealizations made in this study, such as assuming negligible current displacement in the copper windings, are commonly used in simplified models for induction motors (IMs) to reduce computational complexity while maintaining accuracy in most industrial applications. These assumptions are typically valid when the motor operates under standard conditions where current displacement effects are minimal. However, in cases where the motor design or operational environment leads to significant current displacement effects (such as high-frequency operation or specific motor designs), these idealizations may limit the accuracy of the model. For motors where current displacement in the windings plays a more prominent role, more advanced models, which account for these effects, are necessary [50,51].

2.1. Generalized Electric Machine Equations

Generalized electric machine equations are a system of differential equations that include the equilibrium equations for the windings voltages of machine and the equation of motion (torque balance equation on the machine shaft). The rotor windings' parameters are reduced to the stator windings (with the reduction marks omitted).

Thus, on axes 1α , 1β and 2α , 2β [49]:

$$U_{1\alpha} = R_1 i_{1\alpha} + \frac{d}{dt} \psi_{1\alpha}; \quad (1)$$

$$U_{1\beta} = R_1 i_{1\beta} + \frac{d}{dt} \psi_{1\beta}; \quad (2)$$

$$U_{2\alpha} = R_2 i_{2\alpha} + \frac{d}{dt} \psi_{2\alpha}; \quad (3)$$

$$U_{2\beta} = R_2 i_{2\beta} + \frac{d}{dt} \psi_{2\beta}. \quad (4)$$

In these equations, the flux linkages of the windings are represented as follows:

$$\psi_{1\alpha} = L_{1\alpha} i_{1\alpha} + M_{1\alpha 2\alpha} i_{2\alpha} + M_{1\alpha 2\beta} i_{2\beta} \quad (5)$$

$$\psi_{1\beta} = L_{1\beta} i_{1\beta} + M_{1\beta 2\alpha} i_{2\alpha} + M_{1\beta 2\beta} i_{2\beta} \quad (6)$$

$$\psi_{2\alpha} = L_{2\alpha} i_{2\alpha} + M_{2\alpha 1\alpha} i_{1\alpha} + M_{2\alpha 1\beta} i_{1\beta} \quad (7)$$

$$\psi_{2\beta} = L_{2\beta} i_{2\beta} + M_{2\beta 1\alpha} i_{1\alpha} + M_{2\beta 1\beta} i_{1\beta} \quad (8)$$

where $U_{1\alpha}$, $U_{1\beta}$, $U_{2\alpha}$, $U_{2\beta}$ —are the voltages applied to the machine windings; $i_{1\alpha}$, $i_{1\beta}$, $i_{2\alpha}$, $i_{2\beta}$ are the currents in the windings;

R_1, R_2 are the resistances in stator and rotor windings, respectively;
 $L_{1\alpha}, L_{1\beta}, L_{2\alpha}, L_{2\beta}$ —are the self-induction inductances of the stator and rotor windings;
 $M_{1\alpha 2\alpha}, M_{1\alpha 2\beta}, M_{1\beta 2\beta}, M_{1\beta 2\alpha}, M_{2\alpha 1\alpha}, M_{2\alpha 1\beta}, M_{1\beta 2\beta}, M_{2\beta 1\beta}$ are the mutual inductances between the stator and rotor windings.

Since the air gap of the machine is constant along the stator circumference and the magnetic field is not saturated, the self-inductance coefficients $L_{1\alpha}, L_{1\beta}, L_{2\alpha}, L_{2\beta}$ are constant.

The symmetry of the machine along the α, β axes and the sinusoidal distribution of the winding magnetomotive force allow us to establish the following equalities:

$$\begin{aligned} M_{1\alpha 2\alpha} &= M_{2\alpha 1\alpha} = M_{1\beta 2\beta} = M_{2\beta 1\beta} = M \cdot \gamma; \\ M_{1\alpha 2\beta} &= M_{2\beta 1\alpha} = -M \cdot \sin \gamma; \\ M_{1\beta 2\alpha} &= M_{2\alpha 1\beta} = M \cdot \sin \gamma; \end{aligned}$$

where M —mutual inductance coefficient when windings axes have a specific angle.

Rotor movement equation:

$$T_e = T_l + J \frac{d\Omega}{dt}, \tag{9}$$

where T_e —developed by machine electromagnetic torque;

T_l —load torque;

$J \frac{d\Omega}{dt}$ —dynamic torque;

J is the combined inertia of the rotor and the equipment inertia, reduced to the rotor shaft;
 Ω —rotation speed, and when $2p = 2$, where p is the number of pole pairs, $\Omega = \omega$ (for generalized electric machine).

The equations fully define dynamic and static processes in generalized electric machine.

Given \dot{U}_1 for stator winding and \dot{U}_2 for the rotor winding:

$$\dot{U}_1 = U_{1m} \cdot e^{j(\omega_1 t + \alpha_0)} = U_{1m} [\cos \cos (\omega_1 t + \alpha_0) + j \sin \sin (\omega_1 t + \alpha_0)] \tag{10}$$

$$\dot{U}_2 = U_{2m} \cdot e^{j(\omega_2 t + \alpha_2)} = U_{2m} [\cos \cos (\omega_2 t + \alpha_2) + j \sin \sin (\omega_2 t + \alpha_2)] \tag{11}$$

In these equations:

ω_1 —angular rotation speed of network;

ω_2 —angular rotation speed of vector \dot{U}_2 comparing to rotor axes;

α_0 —phase angle of vector \dot{U}_1 relative to the axis 1α at the time point $t = 0$;

α_2 —phase angle of vector \dot{U}_2 relative to the axis 2α at the time point $t = 0$.

Obviously, the system of differential Equations (1)–(4) and (9) becomes cumbersome due to periodic coefficients. Additionally, the coefficients of the current in the flux linkages are variable functions, making these equations extremely challenging to solve. This complexity arises from the large number of variables, nonlinearities, and complex physical interactions that characterize the processes in a multiphase machine. To make the problem more manageable, the machine is transformed into a two-phase model, significantly reducing the number of equations and simplifying their solution [49].

The coordinate system $1\alpha, 1\beta$ is stationary, while the coordinate system $2\alpha, 2\beta$ rotates with rotor’s angular speed ω .

2.2. Generalized Machine in Common Coordinates Axes Rotating at Arbitrary Speed

To simplify the analysis of an electric machine, we aim to make the magnetic fields of the stator and rotor appear stationary relative to each other. This can be achieved in two ways:

- Braking the rotor’s rotating windings: this means that, from a mathematical perspective, we adjust the reference frame so that the rotor’s windings appear stationary, even though they are physically rotating;

or

- Rotating the stator’s windings at the same speed as the rotor: in this case, we imagine that the stator windings are rotating at the same speed as the rotor, effectively making the stator and rotor fields appear stationary relative to each other.

In both scenarios, we must adjust the frequency of the currents in the windings to reflect this new reference frame, where the fields are stationary. To account for this, an electromotive rotational force is introduced into the voltage and current equations. This adjustment ensures that the real electrical behavior of the machine is accurately captured in the equations.

Next, we convert the system of equations into the x, y coordinate system, which rotates at an arbitrary speed. This common coordinate system simplifies the analysis and makes it easier to model the dynamics of the machine (see Figure 1).

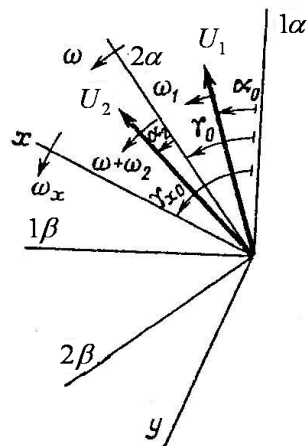


Figure 1. Coordinate system and voltages space vectors.

The stator-winding voltage balance equation expressed using space vectors $\dot{U}_1; \dot{\psi}_1; \dot{I}_1$ is

$$\dot{U}_1 = R_1 \dot{I}_1 + \frac{d\dot{\psi}_1}{dt}.$$

Thus, equation should be multiplied by $e^{-j(\omega_x t + \gamma_{x0})}$. This multiplier accounts for the rotation frequency difference between the stationary $1\alpha, 1\beta$ coordinate system and the rotating x, y coordinate system.

$$\dot{\psi}_1(x, y) = \dot{\psi}_1 e^{-j(\omega_x t + \gamma_{x0})} = \dot{\psi}_{1m} e^{j((\omega_1 - \omega_x)t + \alpha_0 - \gamma_{x0} - \phi)}; \tag{12}$$

$$\begin{aligned} \dot{U}_1(x, y) &= \dot{U}_1 \cdot e^{-j(\omega_x t + \gamma_{x0})} = U_{1m} \cdot e^{j(\omega_1 t + \alpha_0)} \cdot e^{-j(\omega_x t + \gamma_{x0})} = \\ &= U_{1m} \cdot e^{j((\omega_1 - \omega_x)t + \alpha_0 - \gamma_{x0})}; \end{aligned} \tag{13}$$

$$\dot{I}_1(x, y) = \dot{I}_1 e^{-j(\omega_x t + \gamma_{x0})} = I_{1m} \cdot e^{j((\omega_1 - \omega_x)t + \alpha_0 - \gamma_{x0} - \phi)}. \tag{14}$$

where ϕ is the angle of displacement between the vectors, $\dot{\psi}_1, \dot{I}_1$ relative to \dot{U}_1 at the time point $t = 0$.

The derivative:

$$\begin{aligned} \frac{d\dot{\psi}_1(x, y)}{dt} &= \frac{d}{dt} \left\{ \dot{\psi}_1 \cdot e^{-j(\omega_x t + \gamma_{x0})} \right\} \\ &= \left(\frac{d\dot{\psi}_1}{dt} \right) \cdot e^{-j(\omega_x t + \gamma_{x0})} - j\omega_x \dot{\psi}_1 e^{-j(\omega_x t + \gamma_{x0})}. \end{aligned} \tag{15}$$

From this, we obtain the following:

$$\dot{U}_1(x, y) = R_1 \dot{I}_1(x, y) + \frac{d\dot{\psi}_1(x, y)}{dt} + j\omega_x \dot{\psi}_1(x, y). \tag{16}$$

The real and imaginary parts of this equation yield the voltage balance equations in the x, y axes:

$$U_{1x} = \frac{d\psi_{1x}}{dt} - \omega_x \psi_{1y} + R_{1y} + R_1 i_{1x} \quad U_{1y} = \frac{d\psi_{1y}}{dt} - \omega_x \psi_{1x} + R_{1y} + R_1 i_{1y} \quad (17)$$

Similarly, the voltage balance equation for the rotor windings is the following:

$$\dot{U}_2 = \frac{d\psi_2}{dt} + R_2 \dot{I}_2 .$$

Multiplying by $e^{-j((\omega-\omega_k)t+\gamma_0-\gamma_{x0})}$ accounts for the relative difference in rotation speed between the $2\alpha, 2\beta$ and x, y coordinate systems.

Applying analogous transformations as for the stator equations, we obtain the following:

$$\dot{U}_2(x, y) = \frac{d\psi_2(x, y)}{dt} + j(\omega - \omega_2)\psi_2(x, y) + R_2 \dot{I}_2(x, y). \quad (18)$$

Transforming the generalized electric machine equations into a coordinate system that is common for both the stator and rotor and rotates with the free rotation frequency, we obtain the voltage balance equations in the x, y axes.

$$U_{2x} = \frac{d\psi_{2x}}{dt} - (\omega - \omega_x)\psi_{2y} + R_2 i_{2x} \quad U_{2y} = \frac{d\psi_{2y}}{dt} - (\omega - \omega_x)\psi_{2x} + R_2 i_{2y} \quad (19)$$

By setting the values of frequencies $\omega_1, \omega_2, \omega$, and ω_x , we can examine the induction machine in any coordinate system.

A notable feature of the derived model is the presence of rotation electromotive forces: $\omega_x \psi_{1y}, \omega_x \psi_{1x}, (\omega - \omega_x)\psi_{2y}, (\omega - \omega_x)\psi_{2x}$.

In the x, y coordinate system (common to both stator and rotor windings), the machine windings are semi-fixed, meaning that flux linkages of windings lose their alternating coefficients:

$$\begin{aligned} \psi_{1x} &= L_{1x} i_{1x} + L_m i_{2x} \\ \psi_{1y} &= L_{1y} i_{1y} + L_m i_{2y} \\ \psi_{2x} &= L_m i_{1x} + L_{2x} i_{2x} \\ \psi_{1y} &= L_m i_{1y} + L_{2y} i_{2y} \end{aligned}$$

2.3. The Model of Induction Motor in the $\alpha\beta$ Coordinate System

For $\beta (\omega_x = 0)$ —a fixed coordinate system with axes linked to stator-solving Equations (17) and (19) with respect to the derivatives of the flux linkages gives the following form:

$$\begin{aligned} \frac{d\psi_{1\alpha}}{d\tau} &= U_m \cos(\tau) - R_1 i_{1\alpha} \quad \frac{d\psi_{1\beta}}{d\tau} = U_m \cos(\tau) - R_1 i_{1\beta} \quad \frac{d\psi_{2\alpha}}{d\tau} = \\ &-R_2 i_{2\alpha} + \omega \psi_{2\beta} \quad \frac{d\psi_{2\beta}}{d\tau} = -R_2 i_{2\beta} + \omega \psi_{2\alpha} , \end{aligned} \quad (20)$$

The equation for the change in rotor speed is

$$\frac{d\omega}{d\tau} = (T_e - T_l) / T_M, \quad (21)$$

The current values are obtained from flux linkages expressions:

$$\begin{aligned} i_{1\alpha} &= \frac{(X_2 \psi_{1\alpha} - X_{ad} \psi_{2\alpha})}{\Delta} \quad i_{1\beta} = \frac{(X_2 \psi_{1\beta} - X_{ad} \psi_{2\beta})}{\Delta} \quad i_{2\alpha} \\ &= \frac{(X_1 \psi_{2\alpha} - X_{ad} \psi_{1\alpha})}{\Delta} \quad i_{2\beta} = \frac{(X_1 \psi_{2\beta} - X_{ad} \psi_{1\beta})}{\Delta} \end{aligned} \quad (22)$$

where $\Delta = X_1 X_2 - X_{ad} X_{ad}$.

$$T_e = X_{ad}(i_{1\alpha} i_{2\beta} - i_{1\beta} i_{2\alpha}) \quad (23)$$

And the load torque is the following:

$$T_l = SM\omega_2^2 + SMC \quad (24)$$

where:

- $\psi_{1\beta}, \psi_{1\alpha}, \psi_{2\beta}, \psi_{2\alpha}$ are the stator and rotor flux linkage components in the $\alpha\beta$ coordinate system;
- $i_{1x}, i_{1y}, i_{2x}, i_{2y}$ are the stator and rotor current components in the $\alpha\beta$ coordinate system;
- ω is the rotor rotation speed;
- $U_m \cos(\tau), -U_m \sin(\tau)$ are the stator applied voltage;
- $R_1, R_2, X_1, X_2, X_{ad}$ are the induction motor parameters in per units;
- T_e, T_l are the electromagnetic and load torques, respectively;
- SM, SMC are the motor's variable and constant torques coefficients.

Using the developed IM model in the α, β coordinate system, there is an opportunity to model various dynamic operating regimes, such as direct starting, and direct starting considering current displacement in the slots.

This IM model in the α, β coordinate system allows for the direct comparison of single-phase outcomes with experimental data without the need for additional transformations.

3. Modeling the Direct-Starting Mode of an Induction Motor

The direct-starting mode of an IM is a critical stage in its operation, as it determines whether the motor can successfully transition from rest to its steady-state operating condition [37]. The method of starting plays a crucial role in ensuring that the motor operates effectively, and different starting methods are employed depending on the operating conditions and the electrical network requirements [50].

When using direct starting, however, large inrush currents and significant voltage drops in the network can occur, which may reduce the motor's lifespan and affect the stability of the electrical system. During the starting process, the application of voltage to the stator winding induces both harmonic currents and flux linkages corresponding to the applied voltage, as well as transient components. These transients result in complex interactions between the stator and rotor fluxes. With some simplification, it can be assumed that one of the transient fluxes remains stationary relative to the stator, while the other rotates with the rotor. The forced flux rotates at synchronous frequency, and the rotor flux linkage caused by the rotating-free flux decays over time [51,52].

The electromagnetic torque generated during this phase is the result of the interaction of all these fluxes. The transient currents that arise in the stator and rotor windings during the starting process follow complex oscillatory patterns, and the electromagnetic torque they generate is similarly oscillatory and dependent on time [53,54].

Understanding the processes that occur during starting allows for the selection of optimal starting methods to minimize these negative effects [7].

There are two major challenges associated with the direct starting mode of an induction motor (IM): a high starting current, which can be 6–10 times higher than the normal operating current, and fluctuations in the motor's starting torque. These torque fluctuations, or variations, mean that the motor does not produce smooth torque during startup, which can result in vibrations and mechanical stress [6,55,56]. These factors lead to the following consequences:

- The high starting current causes a significant voltage drop on the main substation buses (especially if the transformer and motor power are comparable), which disrupt the operation of other consumers and the motor itself (resulting in a start-up delay).

- The high starting current also induces significant thermal overload on the windings, leading to accelerated aging of the insulation. This ultimately results in insulation breakdown and inter-turn short circuits.
- Large torque fluctuations during the start-up period, which can exceed the nominal torque by 4–5 times, create unfavorable conditions for the mechanical system connected to the motor (such as gears, belts, or shafts), causing stress and potentially damaging these components.

The process of accelerating an IM during starting mode is divided into three stages (Figure 2):

1. Application of voltage to the stator windings, while the rotor is in a fixed position, inducing both forced and transient currents in the windings.
2. The rotor begins to rotate and reaches critical slip, which is the point where the motor produces its maximum torque. This occurs when the rotor speed lags behind the synchronous speed of the magnetic field by an optimal amount before the motor accelerates further.
3. The rotor accelerates from critical slip to a steady rotational speed.

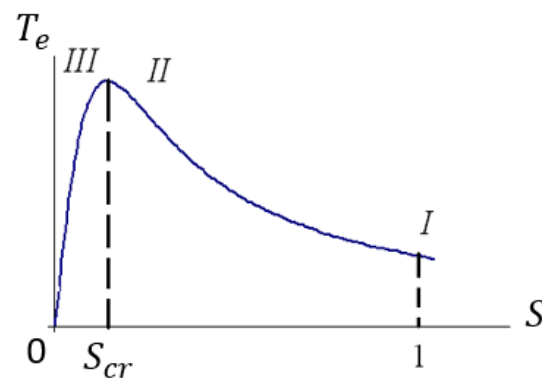


Figure 2. Characteristic stages of the induction motor starting process, where T_e is the electromagnetic torque and S is the slip [57].

For starting-mode modeling, the parameters of 3 kW induction motor with the following per unit (pu) values were used [58]: $X_1 = 0.057$ pu, $X_{ad} = 3.4$ pu, $X_2 = 0.1$ pu, $R_1 = 0.072$ pu, $R_2 = 0.0487$ pu, $T_M = 32.986$.

Figure 3 presents the dynamic characteristics of torque, current, and rotation frequency obtained through mathematical modeling for the direct-starting mode of an IM under no-load operation.

The electromagnetic torque characteristics of an IM during the starting phase are illustrated for different load conditions in Figure 4. The curves correspond to varying load torques represented by the load variables SM and SMC. Specifically, $SM = 0.8$ (pu) represents a variable load, while $SMC = 0.2$ (pu) and $SMC = 0.5$ (pu) represent constant loads on the motor. These characteristics are influenced by different values of the motor's active and reactive resistances. The torque response demonstrates how the motor behaves under these changing load conditions, providing a detailed understanding of its dynamic performance during starting mode.

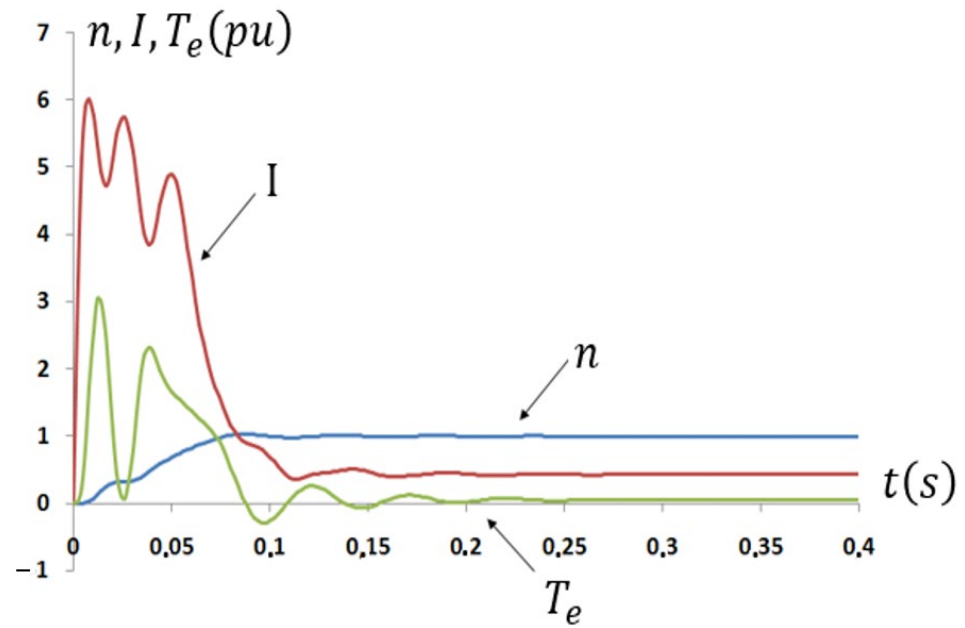


Figure 3. Starting mode of a 3 kW induction motor, where n (rotational frequency), I (current), and T_e (electromagnetic torque) are all expressed in per unit (pu), as a function of time (in seconds).

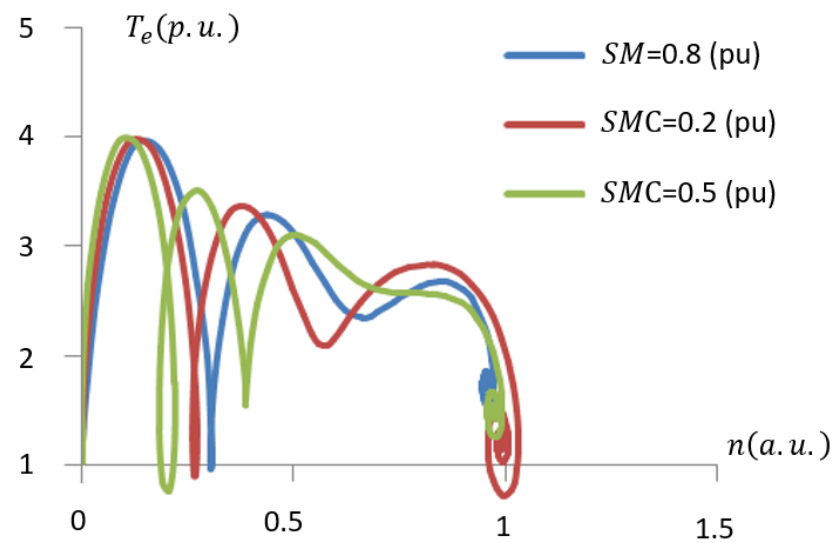


Figure 4. Dynamic characteristics of a 3 kW induction motor during the starting mode, where T_e (electromagnetic torque) and n (rotational speed) are expressed in per units, depending on the induction motor load characteristics.

Figure 5 illustrates the static and dynamic torque characteristics of a 3 kW induction motor during the starting phase. The static characteristic, shown in blue, represents the motor's behavior under steady-state conditions, while the dynamic characteristic, shown in red, is obtained through modeling. As discussed earlier, these characteristics exhibit significant differences, reflecting the complex interactions and transient phenomena that occur during dynamic operation compared to the steady-state performance.

As discussed earlier, these characteristics exhibit significant differences, reflecting the complex interactions and transient phenomena that occur during dynamic operation compared to the steady-state performance.

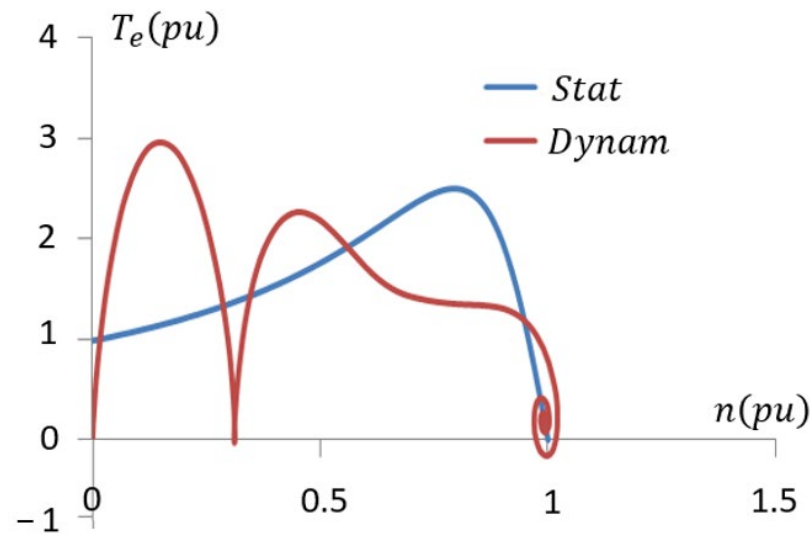


Figure 5. Static and dynamic starting characteristics of a 3 kW induction motor.

4. Modeling the Direct Starting of an Induction Motor with Consideration of Slot Current Displacement

In a squirrel cage induction motor, slots are the grooves in the rotor and stator cores where the conductive bars (in the rotor) and windings (in the stator) are housed. These slots are essential because they guide the flow of electrical current through the motor and contribute to generating the electromagnetic field necessary for its operation.

Changes in the active resistance of the winding can be caused by variations in temperature, current displacement due to frequency changes, and the inclusion of nonlinear resistors. Current displacement in the slot refers to the uneven distribution of electric current within the conductor bars in the rotor slots. This occurs because the inductive reactance of the conductors varies depending on their position within the slot. Conductors located at the bottom of the slot experience different inductive reactance compared to those nearer the air gap. As a result, the current is not uniformly distributed along the slot height.

When the angular velocity of the rotor changes, the frequency of the current in the rotor bars also changes, which further affects the distribution of current density along the conductors inside the slots. This variation in current density leads to changes in both the amplitude and phase of the currents along the slot height.

In most cases, changes in active resistance due to temperature occur slowly and do not significantly affect the motor's dynamic behavior. However, when operating electric converters (ECs)—devices used to control the speed and torque of induction motors by adjusting supply frequency and voltage—the most significant focus is on studying the impact of current displacement in the slots on the motor's dynamic characteristics.

The distribution of current along the slot is illustrated in Figure 6a. The current is distributed unevenly along the width of the slot as well. The coefficient K_r , which accounts for the increase in active resistance due to current displacement, depends on the type of winding, the geometrical data of the slot, the number and sizes of the elementary conductors, and the frequency of the current in them [49]. The leakage inductive reactance also changes due to current displacement. This is accounted for by the coefficient K_x . The coefficients K_r and K_x change according to a nonlinear law as the rotor speed varies. The changes in K_r and K_x in per unit for a deep slot are shown in Figure 6b. By determining the laws of variation for the active and reactive resistances of the slot, the equations of electromechanical energy conversion are modeled, taking into account the changes in the rotor-winding resistances.

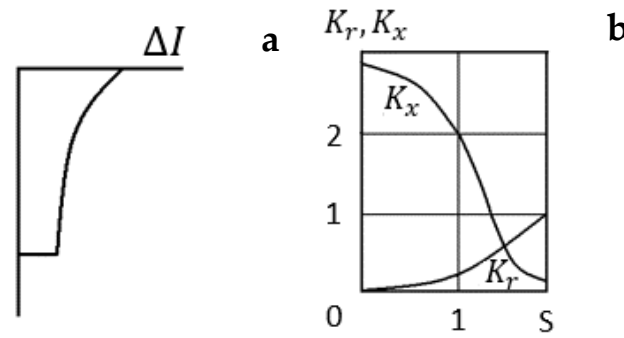


Figure 6. Current distribution along the height of the slot in an electrical machine (a); dependence of K_r and K_x on slip (b).

Research shows that the nonlinear variation of the rotor’s active resistance has the greatest impact on the dynamics during the starting mode of an IM. Due to current displacement in the rotor slots, the acceleration time is reduced, and surge currents and torques are decreased.

The shape of the grooves affects the law of change in K_r and K_x and, consequently, impacts the dynamic characteristics. However, the initial and final values of resistance have a greater influence on the energy conversion processes.

To determine the parameters of resistance, change during the startup of an induction motor, the following expression can be used [59]:

$$Z'_2(s) = \frac{R'_2(s)}{s} + jX'_2(s) \tag{25}$$

where R'_2 , $X'_2(s)$ are rotor parameters that depend on slip, reduced to the stator frequency, i.e., $X'_2(s) = \omega_1 L'_2(s)$.

In all design types of squirrel cage rotors (deep-bar, double-cage, and solid), the active resistance increases with increasing slip, while the reactive resistance decreases. It can be shown that the same approximate formula for parameters as a function of slip is valid for all types of rotors [59].

$$R'_2(s) = R'_{2N} \left[1 + \left(\frac{R'_2(1)}{R'_{2N}} - 1 \right) \sqrt{s} \right] \tag{26}$$

$$X'_2(s) = X'_{2a} \left[1 + \frac{\left(\frac{X'_{2N}}{X'_{2a}} - 1 \right)}{1 + b\sqrt{s}} \right] \tag{27}$$

$$b = \frac{\frac{X'_{2N}-1}{X'_2(1)}}{1 - \frac{X'_{2a}}{X'_2(1)}} \tag{28}$$

where R'_{2N} , $X'_2(1)$ rotor windings’ parameters at slow frequency (practically on nominal slip): $R'_2(1)$, R'_{2N} parameter on slip $s = 1$.

X'_{2a} —the part of reactive rotor winding, which is not depending on slip (differential dispersion or dispersion of crown of tooth, dispersion in the open slot, dispersion of end coil, except the machines with current dispersion in end coil).

Using the IM mathematical model, the starting mode was modeled, taking into account current displacement in slots. The modeling results are presented on Figures 7–9. The curves also reflect the characteristics obtained during starting mode without considering current displacement in the slots, as discussed in the previous chapter.

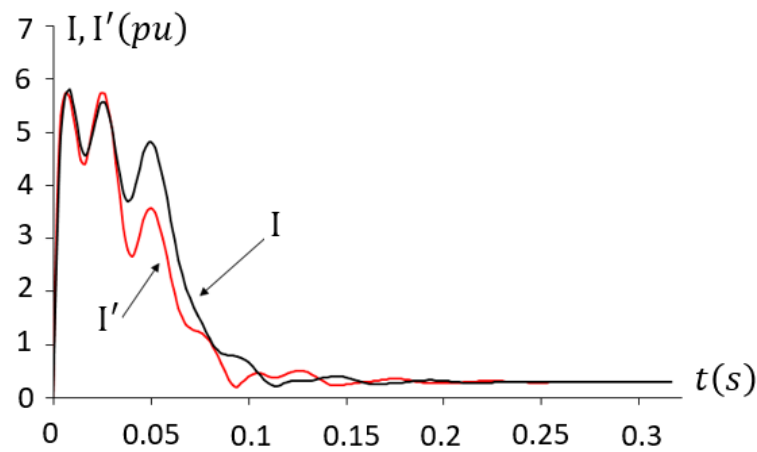


Figure 7. Current change characteristics during IM starting mode. I —starting mode without considering current displacement in slots; I' —starting mode with current displacement in slots.

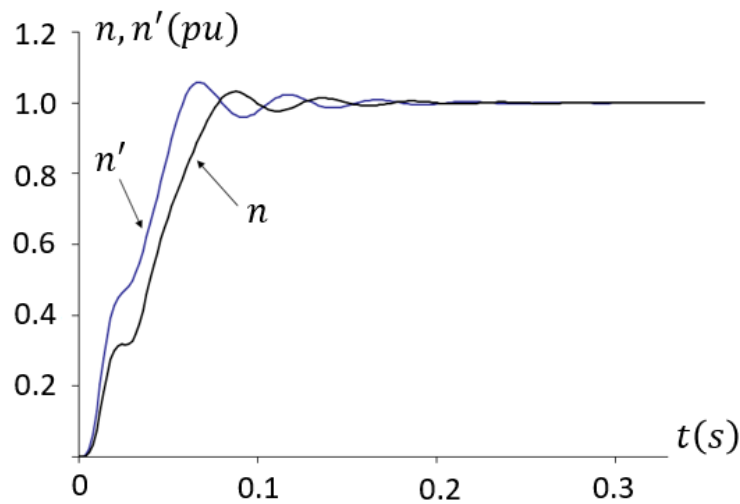


Figure 8. Rotation frequency change characteristics on IM starting mode. n —starting without current displacement in slots. n' —starting mode taking current displacement in the slots.

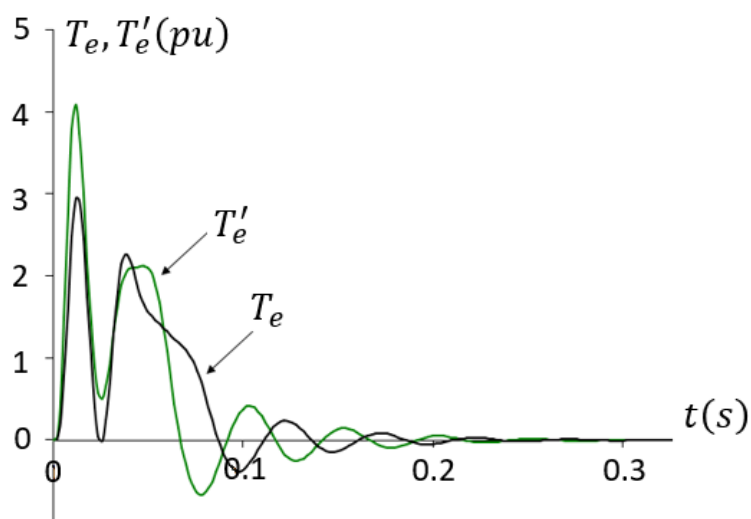


Figure 9. Electromagnetic torque change characteristics during IM starting. T_e —starting without considering current displacement in slots; T_e' —starting with current displacement in slots taken into account.

A comparison of the current characteristics of the IM showed that when considering current displacement in the slot, the starting current of the IM matches the first and second amplitudes of the starting current without considering current displacement in the slot. However, the value of the third amplitude is significantly less than when starting without considering current displacement. Overall, the starting-current characteristic with slot current displacement exhibits a more rapidly decaying nature than the characteristic obtained without considering current displacement. In steady-state mode, the characteristics completely coincide.

From the starting-frequency characteristic of the IM, it is evident that when starting with slot current displacement taken into account, the IM reaches steady-state mode faster than when starting without considering current displacement in the slots. A comparison of the electromagnetic torque characteristics shows that when modeling the start with slot current displacement considered, the first torque amplitude significantly exceeds the value obtained when modeling the IM start without considering slot current displacement. Thus, the conducted study demonstrates that accounting for slot current displacement affects the starting characteristics of current, rotational frequency, and electromagnetic torque of the IM but does not affect the steady-state mode.

5. Comparison of Results Obtained from the Mathematical Model and Experimental Data

The characteristics of current, rotational frequency, and torque obtained using the IM model were compared with experimental data. As described in Section 2.3, the IM model in α, β coordinates allow for the comparison of the results from one of the phases with experimental data without requiring additional transformations. To verify the accuracy of the presented mathematical model of the IM in α, β coordinates and the starting characteristics obtained with its help, an experiment was conducted.

To validate the IM-starting characteristics obtained through mathematical modeling, a test stand was constructed, as shown in Figure 10.



Figure 10. Setup of the induction motor for measuring starting characteristics.

The diagram (Figure 11) illustrates the key components of the test stand used for the experiments, including the induction motor (IM), torque sensor, electromagnetic brake, tachogenerator (TG), and associated measurement equipment. Electrical and mechanical values were measured using MODMECA and MODELEC modules. A HAMEG oscillo-

scope was used for data acquisition, with the data transferred to a data management system for further analysis. The setup is powered by a three-phase AC source, with transformers (TR and ATR) providing necessary adjustments for the measurements.

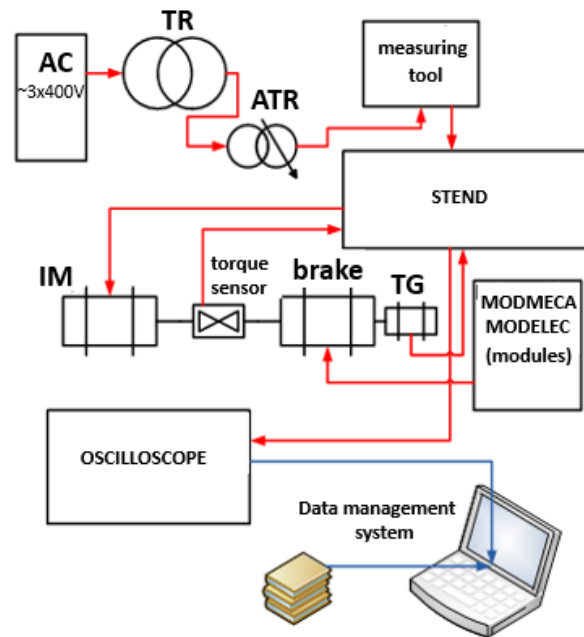


Figure 11. Diagram of the experimental setup for obtaining induction-motor-starting-mode characteristics.

The induction motor’s T-type equivalent circuit is shown in Figure 12 [49]. Table 1 lists the data of the tested IM, while Table 2 presents the data of the IM equivalent circuit (Figure 11) used for modeling [58].

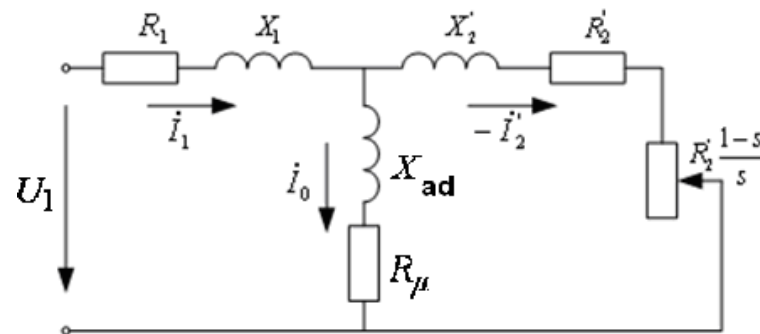


Figure 12. IM T-type equivalent circuit.

Table 1. Technical data of 3 kW IM [58].

P_2 (kW)	U_N (V)	I (A)	$\cos \cos \varphi$	η (%)	f (Hz)	n (min^{-1})
3	220/380	6.1/10	0.88	84.5	50	2840

Table 2. 3 kW IM equivalent circuit catalog data [58].

Motor Type	Equivalent Circuit Parameters (pu) in Nominal Regime					Equivalent Circuit Parameters (pu) at Short Circuit		
	X_{ad}	R'_1	X'_1	R''_2	X''_2	R''_{2start}	$R_{sc,start}$	$X_{sc, start}$
4A90L2Y3	3.4	0.072	0.057	0.047	0.10	0.048	0.12	0.11

Presented below are the current characteristics for one phase, rotational frequency, and electromagnetic torque of the induction motor, obtained both experimentally and through mathematical modeling under no-load operation.

Figure 13 shows a comparison of the phase current I_A of an induction motor obtained by mathematical modeling and the experimentally measured current I_{A_ex} . The graph shows the time evolution of the phase current in per unit (pu) values. Initially, there is a noticeable difference between the modeled and experimental currents during the starting transients, particularly within the first 0.05 s. While the primary focus of this study is on the induction motor's starting process, it is important to highlight that the model has been validated under both transient and steady-state conditions. This comprehensive validation ensures the model's reliability across all phases of motor operation, making it suitable for studying both dynamic (starting) and steady-state conditions.

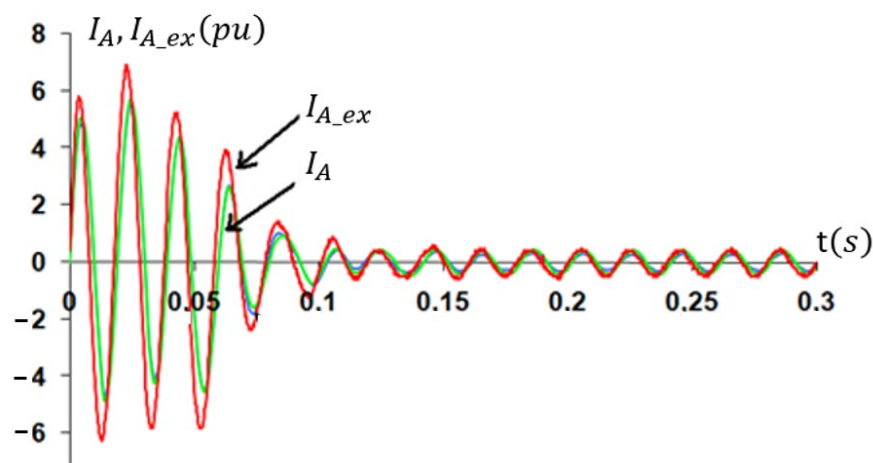


Figure 13. IM-current characteristics obtained through mathematical modeling and experimental measurements.

Figure 14 presents a comparison between the rotational speed n of an induction motor obtained through mathematical modeling and the experimentally measured speed n_{ex} . The graph demonstrates that the modeled and experimental speed curves (n and n_{ex}) are closely aligned throughout the starting phase. Initially, both curves exhibit a rapid acceleration phase, with the motor reaching approximately 80% of its rated speed within the first 0.05 s. After this initial phase, the curves converge almost perfectly, indicating that the mathematical model accurately predicts the motor's dynamic behavior during starting mode. The slight oscillations observed around the steady-state value are minimal and show good agreement between the experimental data and the modeled results.

Figure 15 shows the comparison between the electromagnetic torque T_e of an induction motor obtained through mathematical modeling and the experimentally measured torque T_{e_ex} . The graph illustrates that during the initial starting phase (approximately the first 0.05 s), there is a noticeable difference between the modeled torque T_e and the experimental torque T_{e_ex} . The experimental curve exhibits sharper peaks, indicating transient spikes in the torque that are likely due to real-world factors such as measurement noise, sudden load changes, or mechanical vibrations that are not fully captured by the mathematical model. Despite this initial discrepancy, the curves begin to converge around 0.1 s into the starting process, with the modeled torque aligning closely with the experimental data as the system approaches steady-state operation.

This comparison highlights the effectiveness of the mathematical model in predicting the general trend in the motor's torque response during the starting mode while also underscoring the challenges of accurately modeling the highly dynamic initial transients. The close alignment of the curves after the initial transients suggests that the model is reliable for steady-state analysis and for studying the overall behavior of the motor during the starting phase.

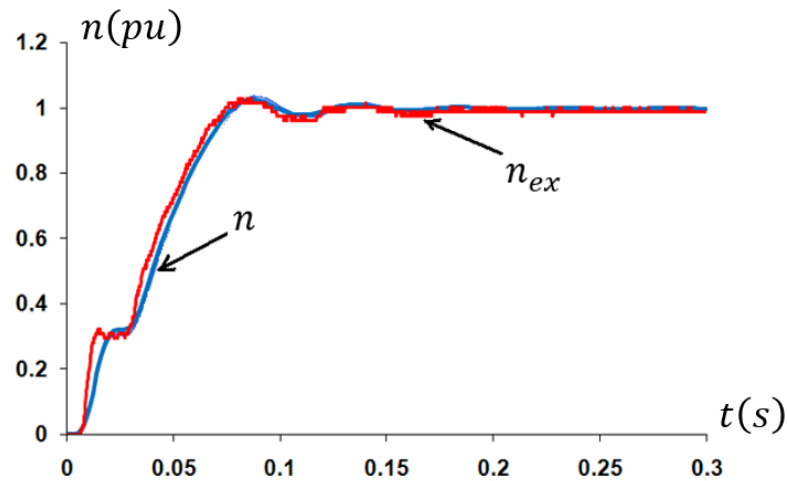


Figure 14. IM-starting characteristics: rotation speed obtained through mathematical modeling and experimental measurements.

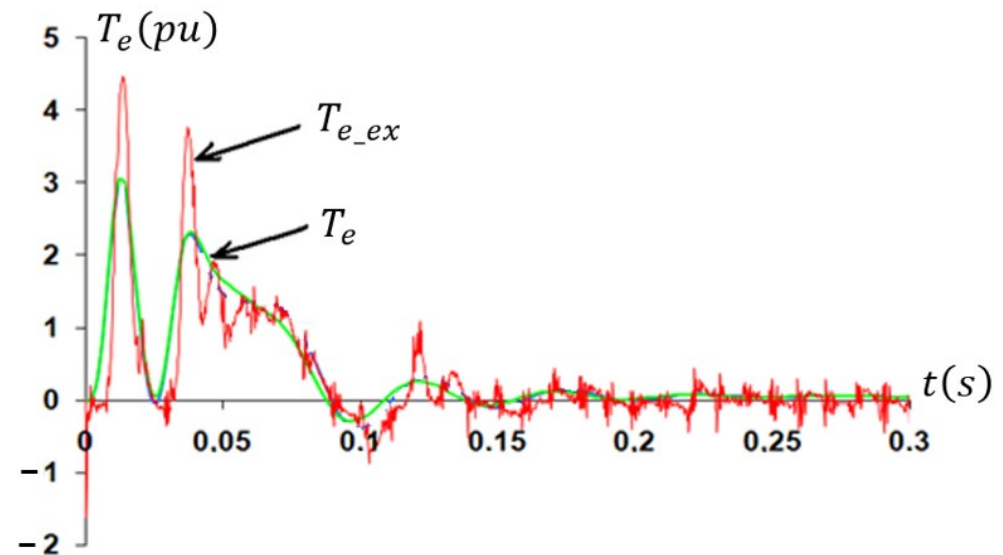


Figure 15. IM-starting characteristics: electromagnetic torque obtained through mathematical modeling and experimental measurements.

6. Discussion

The results obtained from the mathematical modeling of the induction motor's starting behavior provide valuable insights into the transient and steady-state performance of the motor. The developed model, which takes into account current displacement in the rotor slots, shows a significant improvement in the prediction of starting current and torque characteristics. Specifically, the inclusion of current displacement results in a faster transition to steady-state operation and a reduction in the amplitude of the starting current, which are critical factors in enhancing energy efficiency and reducing mechanical stress during startup.

In comparison to the existing literature, traditional models often neglect the current-displacement effect, leading to discrepancies in predicting motor dynamics, particularly during the transient phase. Studies such as those by Kopylov [49] and Krause [54] highlight the challenges of accurately capturing transient phenomena without considering these nonlinear effects. By incorporating current displacement, our model reduces these discrepancies, thus providing a more accurate representation of the induction motor's starting characteristics. Additionally, Menghal et al. [60] discuss various control strategies, including AI-based controllers for improving dynamic response, which also acknowledge

the importance of accurate modeling in transient conditions. Similarly, Larabee et al. [5] emphasize the impact of starting methods on induction motor performance. This research aligns with these studies in recognizing that accounting for complex physical behaviors, such as current displacement, significantly enhances the accuracy of motor simulations, particularly during start-up.

While the model presented in this paper performs well under steady-state conditions and closely aligns with experimental data, certain discrepancies are observed during the initial transient phase. These differences are primarily attributed to model simplifications, such as assuming linear magnetic properties and excluding mechanical factors like friction and vibration. All these limitations have also been noted in previous studies, indicating that the inclusion of these factors could further enhance the model's accuracy.

The comparison between the experimental and simulated data suggests that the proposed model effectively captures the general trends in the motor's behavior, but improvements are needed for better transient accuracy. Future work will focus on incorporating more detailed representations of mechanical losses and magnetic saturation effects to enhance the model's capability in predicting dynamic behavior during motor startup.

7. Conclusions

This paper presents a detailed study of the starting behavior of a three-phase induction motor (IM) with a squirrel cage rotor, using a mathematical model in the α, β coordinate system. The proposed model accurately captures key transient processes, including current, rotational speed, and electromagnetic torque, during the motor's startup phase. The simulation results closely align with experimental data under steady-state conditions, validating the model for practical applications.

A key aspect addressed in this study is the well-established effect of current displacement in the rotor slots. By incorporating this known phenomenon into the model, the starting current and torque profiles were improved, reducing the time to reach steady-state operation. This adjustment results in a lower amplitude of starting current, enhancing the model's reliability for industrial applications where energy efficiency and smooth motor startup are critical.

Despite the model's accuracy in general startup characteristics, discrepancies between the simulated and experimental data during the initial transient phase suggest that additional factors, such as mechanical resonances or nonlinear magnetic effects, may need to be accounted for in future model iterations.

The developed model serves as a strong foundation for analyzing the dynamic behavior of induction motors, especially in startup scenarios without automatic control systems. It offers valuable insights into improving motor performance when current displacement is considered. Future work will focus on refining the model to better capture complex transient phenomena and broadening its application across various industrial settings to optimize energy efficiency and operational reliability.

Funding: M.K. thanks the Institute of Solid State Physics, University of Latvia (ISSP UL), which is as the Center of Excellence is supported through the European Union's Horizon 2020 Framework Programme H2020-WIDESPREAD-01-2016-2017-TeamingPhase2 under grant agreement No. 739508, project CAMART2.

Institutional Review Board Statement: Not applicable.

Informed Consent Statement: Not applicable.

Data Availability Statement: The data and Fortran code supporting the findings of this study are available from the corresponding author upon reasonable request.

Acknowledgments: M.K. thanks Anatoli I. Popov for fruitful discussion.

Conflicts of Interest: The author declares no conflicts of interest.

References

1. Manias, S. *Power Electronics and Motor Drive Systems*; Academic Press: Cambridge, MA, USA, 2016.
2. Emadi, A. *Energy-Efficient Electric Motors, Revised and Expanded*; CRC Press: Boca Raton, FL, USA, 2018.
3. Parekh, R. *AC Induction Motor Fundamentals*; (DS00887A); Microchip Technology Inc.: Chandler, AZ, USA, 2003; pp. 1–24.
4. Gregor, R. (Ed.) *Induction Motors: Applications, Control and Fault Diagnostics*; BoD–Books on Demand; InTech: Rijeka, Croatia, 2015.
5. Larabee, J.; Pellegrino, B.; Flick, B. Induction motor starting methods and issues. In Proceedings of the Record of Conference Papers Industry Applications Society 52nd Annual Petroleum and Chemical Industry Conference, Denver, CO, USA, 12–14 September 2005; pp. 217–222.
6. Kitaneh, A.; Jarrad, A.; Alsadi, S.; Zeidan, A.; Foqha, T.; AlWahhabi, A.; Attar, H. Educational Starting Board for Three-Phase Squirrel Cage Induction Motor. In *Intelligent Systems, Business, and Innovation Research*; Springer Nature: Cham, Switzerland, 2024; pp. 669–680.
7. Singh, I. *Principles of Motor Starting*; Pencil: Mumbai, India, 2024.
8. Zamani, S.Z. Small and Medium Enterprises (SMEs) facing an evolving technological era: A systematic literature review on the adoption of technologies in SMEs. *Eur. J. Innov. Manag.* **2022**, *25*, 735–757. [[CrossRef](#)]
9. Umar, M.F.; Akbar, M.N.; Kazmi, S.M.R. Design and simulation of a 3 phase induction motor drive based on indirect rotor field orientation using MATLAB Simulink tool. In Proceedings of the 2018 1st International Conference on Power, Energy and Smart Grid (ICPESG), Mirpur Azad Kashmir, Pakistan, 9–10 April 2018; pp. 1–6.
10. Prakash, V.; Baskar, S.; Sivakumar, S.; Krishna, K.S. A novel efficiency improvement measure in three-phase induction motors, its conservation potential and economic analysis. *Energy Sustain. Dev.* **2008**, *12*, 78–87. [[CrossRef](#)]
11. Prince Hati, A.S.; Chakrabarti, P.; Abawajy, J.H.; Keong, N.W. Development of energy efficient drive for ventilation system using recurrent neural network. *Neural Comput. Appl.* **2021**, *33*, 8659–8668. [[CrossRef](#)]
12. Le Roux, P.F.; Ngwenyama, M.K. Static and Dynamic simulation of an induction motor using Matlab/Simulink. *Energies* **2022**, *15*, 3564. [[CrossRef](#)]
13. Benninger, M.; Liebschner, M. Optimization of Practicality for Modeling-and Machine Learning-Based Framework for Early Fault Detection of Induction Motors. *Energies* **2024**, *17*, 3723. [[CrossRef](#)]
14. Benninger, M.; Liebschner, M.; Kreischer, C. Fault detection of induction motors with combined modeling-and machine-learning-based framework. *Energies* **2023**, *16*, 3429. [[CrossRef](#)]
15. Rodriguez-Blanco, M.A.; Golikov, V.; Vazquez-Avila, J.L.; Samovarov, O.; Sanchez-Lara, R.; Osorio-Sánchez, R.; Pérez-Ramírez, A. Comprehensive and simplified fault diagnosis for three-phase induction motor using parity equation approach in stator current reference frame. *Machines* **2022**, *10*, 379. [[CrossRef](#)]
16. Sardar, M.U.; Vaimann, T.; Kütt, L.; Kallaste, A.; Asad, B.; Akbar, S.; Kudelina, K. Inverter-Fed Motor Drive System: A Systematic Analysis of Condition Monitoring and Practical Diagnostic Techniques. *Energies* **2023**, *16*, 5628. [[CrossRef](#)]
17. Gundewar, S.K.; Kane, P.V. Condition monitoring and fault diagnosis of induction motor. *J. Vib. Eng. Technol.* **2021**, *9*, 643–674. [[CrossRef](#)]
18. Niu, G.; Dong, X.; Chen, Y. Motor Fault Diagnostics Based on Current Signatures: A Review. *IEEE Trans. Instrum. Meas.* **2023**, *72*, 1–19. [[CrossRef](#)]
19. Pusca, R.; Sbaa, S.; Bessous, N.; Romary, R.; Bousseksou, R. Mechanical failure detection in induction motors using stator current and stray flux analysis techniques. *Eng. Proc.* **2022**, *14*, 19. [[CrossRef](#)]
20. Filippetti, F.; Bellini, A.; Capolino, G.A. Condition monitoring and diagnosis of rotor faults in induction machines: State of art and future perspectives. In Proceedings of the 2013 IEEE Workshop on Electrical Machines Design, Control and Diagnosis (WEMDCD), Paris, France, 11–12 March 2013; pp. 196–209.
21. Tang, J.; Chen, J.; Dong, K.; Yang, Y.; Lv, H.; Liu, Z. Modeling and evaluation of stator and rotor faults for induction motors. *Energies* **2019**, *13*, 133. [[CrossRef](#)]
22. Dehina, W.; Boumehraz, M.; Kratz, F. Diagnosis and Detection of Rotor Bars Faults in Induction Motor Using HT and DWT Techniques. In Proceedings of the 2021 18th International Multi-Conference on Systems, Signals & Devices (SSD), Monastir, Tunisia, 22–25 March 2021; pp. 109–115.
23. Pietrzak, P.; Wolkiewicz, M. Fault diagnosis of PMSM stator winding based on continuous wavelet transform analysis of stator phase current signal and selected artificial intelligence techniques. *Electronics* **2023**, *12*, 1543. [[CrossRef](#)]
24. Dişli, F.; Gedikpınar, M.; Sengur, A. Deep transfer learning-based broken rotor fault diagnosis for Induction Motors. *Turk. J. Sci. Technol.* **2023**, *18*, 275–290. [[CrossRef](#)]
25. Souza, M.V.; Lima JC, O.; Roque AM, P.; Riffel, D.B. A novel algorithm to detect broken bars in induction motors. *Machines* **2021**, *9*, 250. [[CrossRef](#)]
26. Khan, M.A.; Asad, B.; Vaimann, T.; Kallaste, A. An Advanced Diagnostic Approach for Broken Rotor Bar Detection and Classification in DTC Controlled Induction Motors by Leveraging Dynamic SHAP Interaction Feature Selection (DSHAP-IFS) GBDT Methodology. *Machines* **2024**, *12*, 495. [[CrossRef](#)]
27. Wang, W.; Song, X.; Liu, G.; Chen, Q.; Zhao, W.; Zhu, H. Induction motor broken rotor bar fault diagnosis based on third-order energy operator demodulated current signal. *IEEE Trans. Energy Convers.* **2021**, *37*, 1052–1059. [[CrossRef](#)]

28. Hernandez-Ramirez, V.; Almanza-Ojeda, D.L.; Cardenas-Cornejo, J.J.; Contreras-Hernandez, J.L.; Ibarra-Manzano, M.A. Detection of broken bars in induction motors using histogram analysis of current signals. *Appl. Sci.* **2023**, *13*, 8344. [[CrossRef](#)]
29. Chen, L.; Shen, J.; Xu, G.; Chi, C.; Feng, Q.; Zhou, Y.; Deng, Y.; Wen, H. Induction Motor Stator Winding Inter-Tern Short Circuit Fault Detection Based on Start-Up Current Envelope Energy. *Sensors* **2023**, *23*, 8581. [[CrossRef](#)]
30. Sivaraju, S.S.; Senthilkumar, T.; Sankar, R.; Anuradha, T.; Usha, S.; Musirin, I.B. Improving the efficiency of induction motor drive by flux and torque control: A hybrid LSE-RERNN approach. *ISA Trans.* **2024**, *147*, 215–226. [[CrossRef](#)]
31. Aziz AG, M.A.; Abdelaziz, A.Y.; Ali, Z.M.; Diab, A.A.Z. A comprehensive examination of vector-controlled induction motor drive techniques. *Energies* **2023**, *16*, 2854. [[CrossRef](#)]
32. Udomsuk, S.; Areerak, K.; Areerak, T.; Areerak, K. Online Estimation of Three-Phase Induction Motor Parameters Using an Extended Kalman Filter for Energy Saving. *Energies* **2024**, *17*, 2115. [[CrossRef](#)]
33. Konda, Y.R.; Ponnaganti, V.K.; Reddy PV, S.; Singh, R.R.; Mercorelli, P.; Gundabattini, E.; Solomon, D.G. Thermal Analysis and Cooling Strategies of High-Efficiency Three-Phase Squirrel-Cage Induction Motors—A Review. *Computation* **2024**, *12*, 6. [[CrossRef](#)]
34. Yazdi, M. Maintenance strategies and optimization techniques. In *Advances in Computational Mathematics for Industrial System Reliability and Maintainability*; Springer Nature: Cham, Switzerland, 2024; pp. 43–58.
35. Apstein, M.; Blum, L.M. Low-inertia induction motors. *Transactions of the American Institute of Electrical Engineers. Part III Power Appar. Syst.* **1957**, *76*, 253–257.
36. Sen, P.C. *Principles of Electric Machines and Power Electronics, International Adaptation*; John Wiley & Sons: Hoboken, NJ, USA, 2021.
37. Malyar, V.S.; Hamola, O.Y.; Maday, V.S.; Vasylychshyn, I.I. Mathematical modelling of starting modes of induction motors with squirrel-cage rotor. *Electr. Eng. Electromechanics* **2021**, *2*, 9–15. [[CrossRef](#)]
38. Belbali, A.; Makhloufi, S.; Kadri, A.; Abdallah, L.; Seddik, Z. Mathematical Modeling of a Three-Phase Induction Motor. In *Induction Motors-Recent Advances, New Perspectives and Applications*; Intech Open: London, UK, 2023.
39. Dorji, P.; Subba, B. DQ mathematical modelling and simulation of three-phase induction motor for electrical fault analysis. *Int. Adv. Res. J. Sci. Eng. Technol.* **2020**, *7*, 38–46. [[CrossRef](#)]
40. Lin, W.M.; Su, T.J.; Wu, R.C. Parameter identification of induction machine with a starting no-load low-voltage test. *IEEE Trans. Ind. Electron.* **2011**, *59*, 352–360. [[CrossRef](#)]
41. Melkebeek, A.J. *Electrical Machines and Drives: Fundamentals and Advanced Modelling*; Springer International Publishing: New York, NY, USA, 2018.
42. Lee, R.J.; Pillay, P.; Harley, R.G. D, Q reference frames for the simulation of induction motors. *Electr. Power Syst. Res.* **1984**, *8*, 15–26. [[CrossRef](#)]
43. Okpo, E.E.; Le Roux, P.F.; Nnachi, A.F. Induction Motor Fault Identification using Support Vector Machine. In Proceedings of the 2023 6th International Conference on Renewable Energy and Power Engineering (REPE), Beijing, China, 15–17 September 2023; pp. 168–174. [[CrossRef](#)]
44. Oluwasogo, E.S.; Okakwu, I.K.; Ade-Ikuesan, O.O.; Suleiman, H.O. Dq Modelling and Dynamic Characteristics of a Three-Phase Induction Machine. *Am. J. Eng. Res. (AJER)* **2017**, *6*, 207–215.
45. Kidd, B. Vector-Based Magnetic Circuit Modelling of Induction Motors. *Magnetism* **2022**, *2*, 130–151. [[CrossRef](#)]
46. Muchande, S.; Kadam, A.; Unni, K.; Thale, S. Design and implementation of a direct torque control space vector modulated three phase induction motor drive. In Proceedings of the International Conference on Advances in Computing, Communication and Control, Mumbai India, 18–19 January 2013; Springer: Berlin/Heidelberg, Germany; pp. 659–672.
47. Fachini, F.; de Castro, M.; Bogodorova, T.; Vanfretti, L. Modeling of Induction Motors and Variable Speed Drives for Multi-Domain System Simulations Using Modelica and the OpenIPSL Library. *Electronics* **2024**, *13*, 1614. [[CrossRef](#)]
48. Oberkampff, W.L. Simulation accuracy, uncertainty, and predictive capability: A physical sciences perspective. In *Computer Simulation Validation: Fundamental Concepts, Methodological Frameworks, and Philosophical Perspectives*; Springer: Cham, Switzerland, 2019; pp. 69–97.
49. Kopylov, I.P. *Mathematical Models of Electric Machines*; Mir Publishers: Moscow, Russia, 2001; p. 155.
50. Boldea, I.; Nasar, S.A. *The Induction Machine Handbook*; CRC Press: Boca Raton, FL, USA, 2002.
51. Vas, P. *Electrical Machines and Drives: A Space-Vector Theory Approach*; Oxford University Press: Oxford, UK, 1992.
52. McElveen, R.F.; Toney, M.K. Starting high-inertia loads. *IEEE Trans. Ind. Appl.* **2001**, *37*, 137–144. [[CrossRef](#)]
53. Bose, B.K. Power electronics and motor drives recent progress and perspective. *IEEE Trans. Ind. Electron.* **2008**, *56*, 581–588. [[CrossRef](#)]
54. Krause, P.C. Analysis of Electric Machinery and Drive Systems. *IEEE Press Google Sch.* **2002**, *2*, 203–210.
55. Habyarimana, M.; Dorrell, D.G. Methods to reduce the starting current of an induction motor. In Proceedings of the 2017 IEEE International Conference on Power, Control, Signals and Instrumentation Engineering (ICPCSI), Chennai, India, 21–22 September 2017; pp. 34–38.
56. Knežević, I.; Čalasan, M.; Dlabáč, T. Novel Analytical Approaches for Induction Machine Direct Start-up Speed–Time Curve Modeling under Fan Load. *Electr. Eng.* **2024**, *106*, 1925–1938. [[CrossRef](#)]
57. Kasatkin, A.S.; Nemtsov, M.V. *Elektrotehnika [Electrical Engineering]*; Academia Publishing: Los Angeles, CA, USA, 2008.
58. Sobolevskaya, A.E.; Shlaf, M.M.; Afonin, V.I.; Sobolevskaya, E.A. *Asynchronous Motors of the 4A Series: Handbook*; Energoizdat: Moscow, Russia, 1982.

59. Postnikov, I.M. *Obshchaya Teoriya i Perekhodnye Protsessy Elektricheskikh Mashin [General Theory and Transients of Electrical Machines]*; Tekhnika: Kiev, Ukraine, 1966.
60. Menghal, P.M.; Laxmi, A.J. Dynamic modeling, simulation & analysis of induction motor drives. In Proceedings of the 2014 International Conference on Science Engineering and Management Research (ICSEMR), Chennai, India, 27–29 November 2014; pp. 1–7.

Disclaimer/Publisher’s Note: The statements, opinions and data contained in all publications are solely those of the individual author(s) and contributor(s) and not of MDPI and/or the editor(s). MDPI and/or the editor(s) disclaim responsibility for any injury to people or property resulting from any ideas, methods, instructions or products referred to in the content.